**J. Cent. South Univ.** (2013) 20: 2753−2762
**DOI:** 10.1007/s11771-013-1794-2

Springer

# Simulation modeling and experimental analysis of thermodynamic charge performance in a variable-mass thermodynamic system

HU Ji-min(胡继敏), JIN Jia-shan(金家善), YAN Zhi-teng(严志腾)

College of Naval Architecture and Power Engineering, Naval University of Engineering, Wuhan 430033, China



**Abstract:** The thermodynamic charge performance of a variable-mass thermodynamic system was investigated by the simulation modeling and experimental analysis. Three sets of experiments were conducted for various charge time and charge steam flow under three different control strategies of charge valve. Characteristic performance parameters from the average sub-cooled degree and the charging energy coefficient point of views were also defined to evaluate and predict the charge performance of system combined with the simulation model and experimental data. The results show that the average steam flow reflects the average sub-cooled degree qualitatively, while the charging energy coefficients of 74.6%, 69.9% and 100% relate to the end value of the average sub-cooled degree at 2.1, 2.9 and 0 respectively for the three sets of experiments. The mean and maximum deviations of the results predicted from those by experimental data are smaller than 6.8% and 10.8%, respectively. In conclusion, the decrease of average steam flow can effectively increase the charging energy coefficient in the same charge time condition and therefore improve the thermodynamic charge performance of system. While the increase of the charging energy coefficient by extending the charge time needs the consideration of the operating frequency for steam users.

**Key words:** variable-mass thermodynamic system; steam accumulator; thermal mixing; simulation

## 1 Introduction

The variable-mass thermodynamic system, which is critical for converting the ability of lower steam supply to higher steam supply, consists of superheated steam source, steam accumulator, charge control valve and the steam pipes connecting them. The steam accumulator offers the steam of required pressure and quantity for instantaneous consumption of steam users in an extremely short charge time, and the storage mode is similar to that of the conventional industrial wet steam accumulator [1−4].

For the storage of sensible heat in pressurized liquid water, the non-uniformity of temperature distribution in the liquid space of steam accumulator has influence on the energy storage capacity during the charge process. The study of temperature non-uniformity requires the knowledge of thermal and hydrodynamic behavior of thermal stratification inside the liquid space, which includes heat loss to the surrounding environment and thermal mixing in the steam accumulator. The degradation and destruction of the thermal stratification is attributed mainly to the mixing factors [5−7] such as 1) natural convection between hot and cold layers, 2) water recirculation caused by vertical wall conduction, and 3) force convection flow during charge process. The effect of the first and second factors can be minimized by inner insulation while the effect of last one that plays a leading role is difficult to control and to evaluate.

Due to the thermal mixing of forced convection flow between the superheated steam out of boiler and the lower temperature saturation water in the liquid space of steam accumulator, the completeness and quickness of mixing process have direct influences on the temperature non-uniformity, and then on the charge performance. The deterioration of mixing condition will greatly increase the un-condensable superheated steam and then promote the pressure of vapor space up to the preset-value, which leads to the end of charge process prematurely. Meanwhile, because of the temperature non-uniformity, the liquid space is still in a sub-cooled state and the energy storage of steam accumulator cannot probably satisfy the demand of the steam users. In summary, the temperature non-uniformity caused by thermal mixing can be evaluated by calculating the average sub-cooled degree in the liquid space of steam accumulator. The thermal analysis of system charge process for the purpose of quantifying the degree of thermal mixing is a worthwhile endeavor since it can contribute greatly to an

**Foundation item:** Project(20080431380) supported by the China Postdoctoral Science Foundation
**Received date:** 2012−05−07; **Accepted date:** 2012−09−11
**Corresponding author:** JIN Jia-shan, Professor, PhD; Tel: +86−27−83443364; E-mail: hujimin85111@sohu.com

efficient way for improving thermodynamic charge performance.

The instant charge process in variable-mass thermodynamic system, relating to the variable-mass flow in two-phase region, the mixed heating between charge steam and liquid water, the variable flow resistance characteristics of steam pipes and the dynamical matching problems between the steam accumulator and control valve, is quite different from the objects studied in many researches [8−10]. Currently, there are no relevant reports on the research yet.

In this work, simulation modeling and experimental analysis of thermodynamic charge performance in system are considered. The main purpose is to determine the thermal behavior of the steam accumulator for the dynamic charge process under the valve control strategy. Characteristic performance parameters from the average sub-cooled degree of water and the charging energy coefficient point of views are defined to evaluate and predict the thermodynamic charge performance of system.

## 2 Object overview

The main components of variable-mass thermodynamic system are shown in Fig. 1. The steam accumulator is a pressure vessel storing hot water and steam for heat storage and release. The lower part of the steam accumulator is a liquid space and the upper part is a vapor space. At runtime, the superheated steam in steam pipes is sprayed from steam source (usually a boiler) into the liquid space through the control valve. After mixing with the liquid water, the water cycle is formed under the double impacts of the steam jet momentum and the pressure difference inside and outside, then heats the wet steam to the required pressure and temperature. In order to secure the pressure of boiler against the great influence of step-changed steam supply during the charge process, a pressure and temperature reduction device is also constructed for releasing the redundant superheated steam of boiler.

During the charge process, the temperature difference between the vapor steam and the liquid water for the temperature non-uniformity increases with increasing the water depth. In complete thermal mixing condition, only a fraction of superheated steam flows into the upper vapor space for increasing pressure, while a majority of that will be condensed to liquid and release the heat energy for heating up the lower liquid space. Consequently, the small temperature difference between the vapor steam and the liquid water improves the thermodynamic charge performance. Whereas, the deterioration of mixing condition will greatly increase the quantity of un-condensable superheated steam and promote the pressure of vapor space to the preset-value, which leads to the end of charge process prematurely and the failure to satisfy the requirement of the steam users.

In conclusion, in the request of completing charge process within a short time and reaching a required steam pressure in the steam accumulator, the evaluation and prediction of thermodynamic charge performance need the simulation modeling and experimental analysis for system.

## 3 Mathematical model and software module

In Fig. 1, $\tau$ is the time variable (s), $P_1$, $T_1$, $h_1$ and $\rho_1$ are the superheated steam pressure (MPa), temperature (K), specific enthalpy (kJ/kg) and density (kg/m$^3$) at cross-section 1−1 from the exit of steam source, respectively. $Q$ and $F$ are the instantaneous charge steam flow (kg/s) and that of accumulation (kg), respectively; $P$ and $T$ are the wet steam pressure and temperature of steam accumulator at cross-section 3−3, respectively; $h$, $\rho$, $V$ and $a$ are the specific enthalpy, density, volume and water filling coefficient of working fluid in steam accumulator, respectively; $T_W$ is the wall temperature of steam accumulator and $T_{iW}$ is that of internal boundary. Superscripts " ′ " and " ″ " represent the liquid and vapor space parameters of wet steam, respectively.

### 3.1 Performance parameters

3.1.1 Effective heating coefficient

The non-uniformity of temperature distribution in the liquid space has influence on the energy storage capacity during the charge process. To compute the

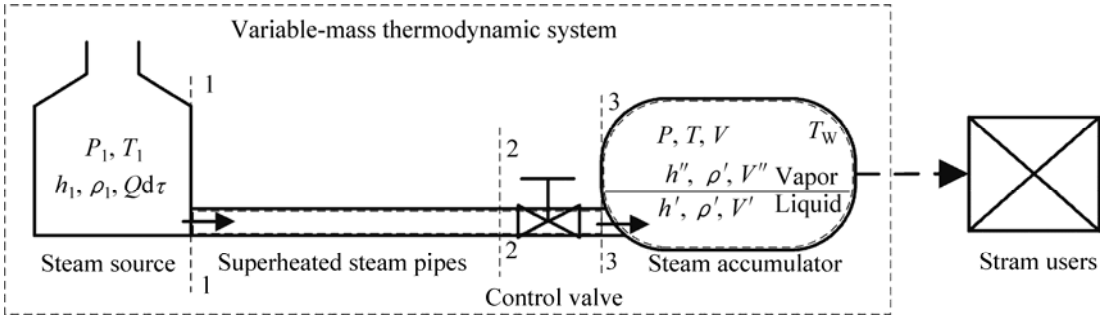


**Fig. 1** Basic structure of variable-mass thermodynamic system

thermal energy accumulated in the liquid space of steam accumulator, the internal energy in the liquid space can be expressed by the volume equivalent $V'_e$ of saturation water under the vapor steam pressure. Thus, the liquid space is assumed to divide into two parts of water layers: one is the upper layer of complete thermal mixing between the superheated steam and the lower temperature saturation water, where the volume is $V'_e$ and the water temperature is equal to the steam temperature $T_{sat}$ under the vapor steam pressure. The other is the lower layer without being involved in the thermal mixing process, where the volume is $V'_a$ and the water temperature is identically equal to the triple point (at the triple point, the water specific internal energy $u_0$=0 kJ/kg). Then, the effective heating coefficient $\phi_e$ is defined as

$$\phi_e = V'_e / V' = V'_e /(V'_e + V'_a) \tag{1}$$

Moreover, it is obtained that $\phi_e$ ($t$=0)=1 since the initial temperature distribution of liquid space is uniform, while $\phi_e \equiv 1$ in an ideal complete mixing condition.

3.1.2 Average sub-cooled degree

The average sub-cooled degree of $\Delta T_{sub}$ evaluates the temperature non-uniformity brought about by thermal mixing of water. It is defined as the temperature difference between the saturation temperature $T_{sat}$ under the vapor steam pressure and the average temperature $T_{sub}$ among the liquid space according to Eq. (2), while the latter can be got with specific internal energy of sub-cooled water $u_{sub}$ by calling the related functions which are based on IAPWS-IF97 (The International Association for the Properties of Water and Steam-Industrial Formulation 1997) for the thermodynamic properties of water and steam [11]:

$$\Delta T_{sub} = T_{sat} - T_{sub} \tag{2}$$

In the steady-state conditions, $u_{sub}$ is calculated as

$$u_{sub} = \frac{\rho' V'_e u' + \rho'_0 (V' - V'_e) u'_0}{\rho' V'_e + \rho'_0 (V' - V'_e)} \tag{3}$$

where $\rho_0$ is the water density at the triple point. Equation (3) is assumed to be also tenable in the dynamic charge conditions [12].

3.1.3 Charging energy coefficient

The thermodynamic charge performance of system is evaluated by calculating the charging energy coefficient $\varphi_i$ in the end of charge process ($t$=$t_{over}$), while $\varphi_i$ is defined as the ratio of the cumulative thermal energy $\Delta E_{act}$ actually delivered by the superheated steam out of the boiler to the thermal energy $\Delta E_{ideal}$ stored by the steam accumulator for reaching the same pressure level in an ideal complete mixing condition, according to Eq. (4):

$$\varphi_i = \frac{\Delta E_{act}}{\Delta E_{ideal}} = \int_0^{t_{over}} h_1 Q_{act} \mathrm{d}\tau \Big/ \int_0^{t_{over}} h_1 Q_{ideal} \mathrm{d}\tau \tag{4}$$

### 3.2 Thermodynamic process model of system

According to the basic working principle of variable-mass thermodynamic system, a mathematical model is established in the allowed scope and following assumptions: Each component is connected in series at the level of system, and the potential energy and kinetic energy of working fluid and the steam leakage during charge process are ignored. Steam accumulator is a rigid storage vessel, of which the vapor steam parameters are treated as lumped parameters, while the liquid space parameter are expressed by the effective heating coefficient in the condition of water layers partition. The heat transfer between the outside wall of steam accumulator and the environment can be neglected for the thick thermal insulation layer. Based on the above assumptions, the model of variable-mass thermodynamic system is established by applying theories of variable-mass thermodynamics and viscous fluid mechanics.

3.2.1 Water/steam module of steam accumulator

Adopting the space in steam accumulator as a control volume for thermodynamic analysis, the state change rule of the working fluid in the control volume simultaneously satisfies the conservation equations of mass, energy and volume [13]:

$$Q\mathrm{d}\tau = \mathrm{d}[(1-\phi_e)V'\rho'_0 + \phi_e V'\rho'] + \mathrm{d}(V''\rho'') \tag{5}$$

$$h_1 \cdot Q\mathrm{d}\tau = \mathrm{d}[(1-\phi_e)V'\rho'_0 u'_0 + \phi_e V'\rho' u'] + \mathrm{d}(V''\rho'' u'') + M_e C_w \mathrm{d}T_{iw} \tag{6}$$

$$V = V'/\alpha = V' + V'' = V'_e/\phi_e + V'' = \text{constant} \tag{7}$$

where $M_e$ and $C_W$ are the effective mass and the heat capacity of metal wall, respectively.

Since the sum of $V'$ and $V''$ is constant in Eq. (7), a hypothetical thermodynamic function $g$ is put forward to eliminate both the differential of $V'$ and $V''$ from Eqs. (5) and (6) and to give the following equations:

$$g \cdot Q - h_1 \cdot Q = g \cdot \sum_{i=1}^{2} \frac{\mathrm{d}f_i}{\mathrm{d}\tau} - \sum_{i=3}^{5} \frac{\mathrm{d}f_i}{\mathrm{d}\tau} = \sum_{j=1}^{8} \left(d_j \cdot \frac{\mathrm{d}W_{je}}{\mathrm{d}\tau}\right) \tag{8}$$

where

$$\boldsymbol{W}_E = [W_{je}]^T = [\rho' \ \ \rho'' \ \ V's \ \ V'' \ \ u' \ \ u'' \ \ \phi_e \ \ T_{iW}]^T$$

$$\boldsymbol{D} = [d_j] = [g \ \ g \ \ -1 \ \ -1 \ \ -1] \cdot \boldsymbol{C}$$

$$\boldsymbol{C} = (\partial f_i / \partial W_{je})_{5\times 8}, (i = 1, 2, \cdots, 5, \quad j = 1, 2, \cdots, 8)$$

$$f_1 = (1-\phi_e)V'\rho'_0 + \phi_e V'\rho'$$

$$f_2 = V''\rho''$$

$$f_3 = (1-\phi_e)V'\rho'_0 u'_0 + \phi_e V'\rho' u'$$

$$f_4 = V''\rho'' u''$$

$$f_5 = M_e C_w \mathrm{d}T_{iw}$$

$$d_1=(g-u')\phi_e V'$$

$$d_2=(g-u'')V''$$

$$d_3=(g-u_0')(1-\phi_e)\rho_0'+(g-u')\phi_e\rho'$$

$$d_4=(g-u_0'')\rho''$$

$$d_5=-\phi_e V'\rho'$$

$$d_6=-V''\rho''$$

$$d_7=V'[(g-u')\rho'-(g-u_0')\rho_0']$$

$$d_8=-M_e C_W$$

It can be observed that the differential of $V'$ and $V''$ are eliminated from Eq. (8) when $d_3=d_4$, that is

$$(g-u_0')(1-\phi_e)\rho_0'+(g-u')\phi_e\rho'-(g-u'')\rho''=0 \tag{9}$$

Consequently, $g$ can be obtained as

$$g=\frac{(1-\phi_e)\rho_0'u_0'+\phi_e\rho'u'-\rho''u''}{(1-\phi_e)\rho_0'+\phi_e\rho'-\rho''} \tag{10}$$

Then put Eq. (10) into Eq. (8) as follows:

$$\sum_{j=1}^{8}\left(d_j\frac{\mathrm{d}W_{je}}{\mathrm{d}\tau}\right)=\left(\frac{(1-\phi_e)\rho_0'u_0'+\phi_e\rho'u'-\rho''u''}{(1-\phi_e)\rho_0'+\phi_e\rho'-\rho''}-h_1\right)\cdot Q=\boldsymbol{d}_k^{\mathrm{T}}\cdot\frac{\mathrm{d}\boldsymbol{W}_{ke}^{\mathrm{T}}}{\mathrm{d}\tau}\ (k=1,2,5,6,7,8) \tag{11}$$

In an ideal complete mixing condition that $\phi_e\equiv 1$, Eq. (11) can be deduced as

$$\begin{aligned}\left(h_1-\frac{\rho'u'-\rho''u''}{\rho'-\rho''}\right)Q=M_e C_W\frac{\partial T_{iw}}{\partial p}\frac{\mathrm{d}p}{\mathrm{d}\tau}+V'\left[\rho'\frac{\partial u'}{\partial p}+\frac{\rho''(u''-u')}{\rho'-\rho''}\cdot\frac{\partial\rho'}{\partial p}\right]\frac{\mathrm{d}p}{\mathrm{d}\tau}+V''\left[\rho''\frac{\partial u''}{\partial p}+\frac{\rho'(u''-u')}{\rho'-\rho''}\cdot\frac{\partial\rho''}{\partial p}\right]\frac{\mathrm{d}p}{\mathrm{d}\tau}\end{aligned} \tag{12}$$

Based on IAPWS-IF97 [11], the characteristic parameters of superheated steam and wet steam can be expressed as

$$h_1=h_1(P_1,T_1),\ \rho_1=\rho_1(P_1,T_1) \tag{13}$$

$$\rho'=\rho'(P),\ h'=h'(P),\ u'=h'-P/\rho' \tag{14}$$

$$\rho''=\rho''(P),\ h''=h''(P),\ u''=h''-P/\rho'' \tag{15}$$

3.2.2 Wall module of steam accumulator

Since the steam accumulator is a thin-walled cylinder, and the $L/D$ ratio is relatively large, the temperature distribution in the cross section of steam accumulator wall changing with the charge process is simplified to an unsteady heat conduction problem of two-dimensional wall with constant properties, isotropic and no internal heat source, which satisfies the parabolic partial differential equation:

$$\frac{1}{r}\frac{\partial}{\partial r}\left(\lambda r\frac{\partial T_w}{\partial r}\right)+\frac{1}{r^2}\frac{\partial}{\partial\varphi}\left(\lambda\frac{\partial T_w}{\partial\varphi}\right)=\rho_w C_w\frac{\partial T_w}{\partial t} \tag{16}$$

where $\rho_W$ is the wall density of metal, kg/m$^3$, and $\lambda$ is the thermal conductivity of metal wall, W/(m·K).

The environmental conditions of the wall can be regarded to be adiabatic. The heat transfer of natural convection and steam condensation, in liquid-wall space and vapor-wall space respectively, are the third type of boundary conditions in the charge process [14]. However, the ratio of liquid space to the total space of the steam accumulator is higher than 80%. In consequence, the heat conduction model is developed in which the coefficient reflecting the effect of mixed convective heat transfer is assumed to natural convection only [13], and the heat transfer between the wall and steam is in line with Neumann boundary conditions:

$$-\lambda\cdot(\partial T/\partial n)=\alpha(T-T_{iw}) \tag{17}$$

where the coefficient of natural convective heat transfer $\alpha$ can be chosen as a constant [15] in the range of 200−1 000 W/(m$^2$·K).

According to Eqs. (1)−(17), there are reciprocal correspondences among $\phi_e$, $P$, $Q$, $P_1$ and $T_1$ during the charge process. Thus, it can be seen that $\phi_e$ can be solved by inputting the experimental data of another four performance parameters to the set of equations of the mathematical model. Moreover, $\Delta T_{sub}$ and $\varphi_i$ can also be calculated after the solution of $\phi_e$.

### 3.3 Simulation model for thermodynamic process of system

The software used to implement the set of equations of the mathematical model and to simulate the dynamic performance of the system is a key feature if the aims of evaluating the performance of the system are to be met. MATLAB/Simulink (specific software for general dynamic systems) was chosen to carry out the modeling task with the discretization and integration method [16−17] based on Eqs. (1)−(17).

The simulation moduli of each subsystem unit in thermodynamic process model are created and connected by MATLAB/Simulink. Figure 2 shows the simulation block diagram which contains the encapsulated subsystem unit of steam accumulator, thermodynamic property of water and steam and input terminal for experimental data.

## 4 Experimental setup

The experimental equipment setup was able to evaluate thermodynamically different characteristic performance parameters that have influence on the system, of which the working fluid is water/steam. The scheme of the system is depicted in Fig. 3. It mainly consists of a full-scale steam accumulator, a boiler for generating superheated steam, a charge control valve, a

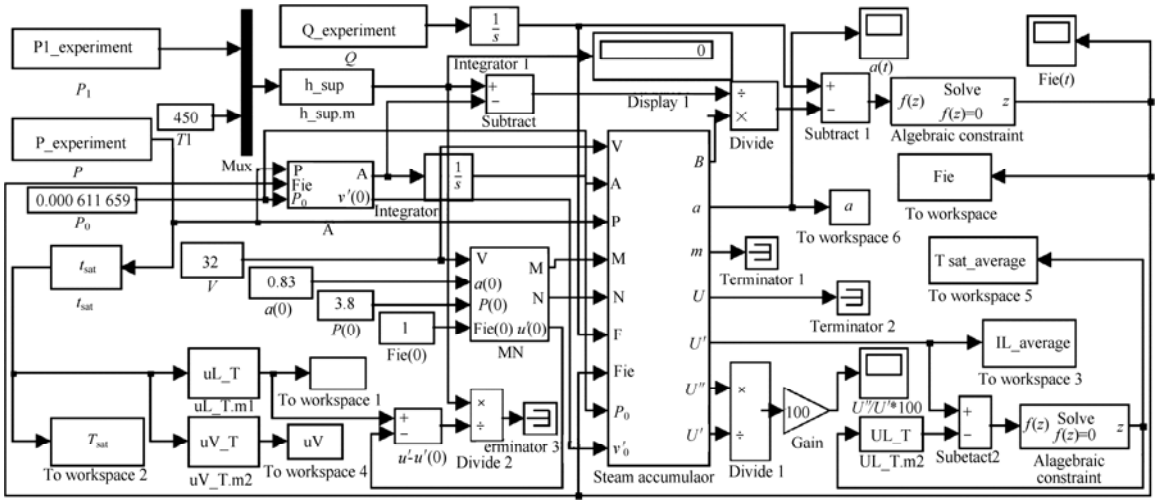


**Fig. 2** System model

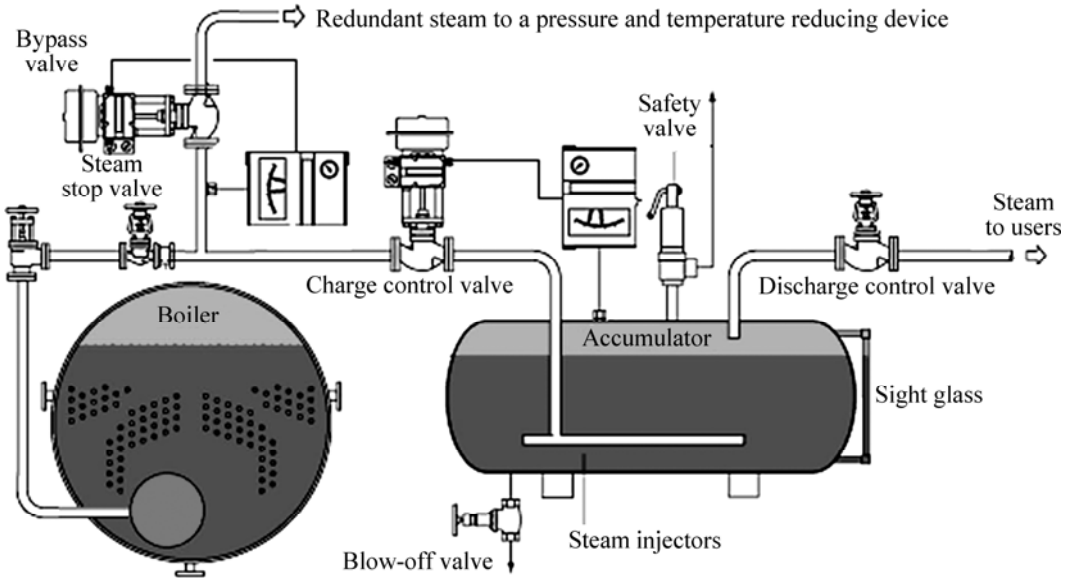


**Fig. 3** Basic structure chart of variable-mass thermodynamic system

pressure and temperature reducing device, a discharge control valve for releasing steam to users, a steam stop valve and other auxiliary components for the steam charge. The experimental prototype has been equipped with a data acquisition system based on PC. In order to carry out the dynamic operation analysis, thermocouples and pressure transducers were placed at the inlet and outlet of each component to determine the steam charge conditions. Given the steam flow was variable during the charge process, the steam flow rate was measured by means of a speed uniform tube type flow meter and an accuracy of 2% of the actual flow rate was achieved by error correction within the operating range.

Steam accumulator is a key part of system which stores thermal energy in the form of hot water during the charge process and delivers it on demand. It consists of a horizontal cylindrical body with a storage capacity of 32 $m^3$ and caps of the hemispherical type made of 85 mm thick stainless steel sheets, as well as a pressure transducer for measuring the pressure of vapor steam. The height and diameter are 8 800 mm and 2 260 mm, respectively.

At runtime, the superheated steam was charged beneath the surface of the water by a distribution manifold, which was fitted with a series of steam injectors for improving thermal mixing process. Obviously, the kind of thermal agitation form is vital to the temperature non-uniformity of liquid space.

Three sets of experiments were conducted for various charge time and charge steam flow under three different control strategies of charge valve (data1, data2 and data3). The differentiation of charge time between data1 and data2 was not so clear. However, the steam flow of the latter was greater than the former during the charge process. Moreover, though the maximum steam flow of data3 was equal to that of data2, the charge time

of the latter was much longer than that of the former. Therefore, three different thermodynamic charge performances of system were tested.

## 5 Results and analysis

### 5.1 Experimental results

The results obtained from three different experiments (data1, data2 and data3) concern the performance parameters of $P_1$, $Q$ and $P$, while $T_1$ is proved to be nearly a constant.

Figure 4 shows the dimensionless steam flow $Q^*$ and accumulation $F^*$ of the system charge process as a function of the dimensionless charge time $t^*$ for three different experiments. These results reflect that the increase of $Q^*$ in the early charge process for data1 and data2 is greater than that for data3. Then, $Q^*$ for data1 and data2 have begun to decrease at $t^*$=0.15, but that for data3 is still increasing. At $t^*$=0.5, though $Q^*$ for data3 decreases with the decrease of charge valve opening, $F^*$ for data3 still excesses that for data1 and data2 because of the both finished charge process. Moreover, these results indicate that the maximum steam flows for data2 and data3 are practically equal to each other which both are 1, while that for data1 is 0.813.

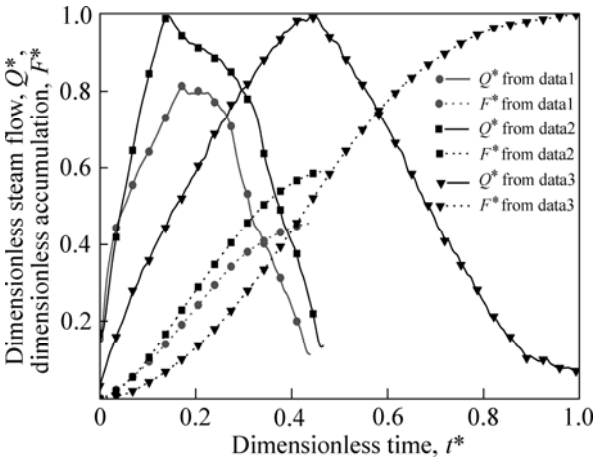


**Fig. 4** Dimensionless steam flow $Q^*$ and accumulation $F^*$ of system charge process as a function of dimensionless charge time $t^*$ for three different experiments (data1, data2 and data3)

Correspondingly, Fig. 5 shows the dimensionless superheated steam pressure $P_1^*$ and specific enthalpy $h_1^*$ of the system charge process as a function of $t^*$ for three different experiments. The deviation amplitude of $P_1^*$ for data1 and data2 that ranges from 0.93 to 1 is much greater than that for data3 with relatively stable pressure, as can be seen in Fig. 5. This effect is also reflected by the evolution of $Q^*$ shown in Fig. 4. When the control for decreasing steam released by the pressure and temperature reduction device cannot keep up with the relatively sharp increase of $Q^*$ for data1 and data2, the increase of steam demand will cause a pressure decrease of superheated steam from boiler. Though $F^*$ for data3 is much greater than both of data1 and data2, the longer charge time results in a relative gentle increase of $Q^*$ so that it doesn't affect the control of the pressure and temperature reduction device, which then brings the relatively stable pressure of superheated steam from boiler. However, it is found that the dimensionless specific enthalpy $h_1^*$ of superheated steam calculated by IAPWS-IF97 [11] has small deviation amplitude, which ranges from 0.968 to 0.97, as also can be seen in Fig. 5.

Figure 6 shows the dimensionless steam pressure $P^*$ of steam accumulator as a function of $t^*$ for three different experiments. These results reflect that there are the consistent variable trend between $P^*$ and $F^*$. The greatest steam flow accumulation for data3 brings the most growth of $P^*$ (ranging from 0.812 to 0.993), the next is data2 (ranging from 0.812 to 0.993) and the last is data1 (ranging from 0.868 to 0.982). Thus, it can confirm that $P^*$ has a certain relationship with $F^*$.

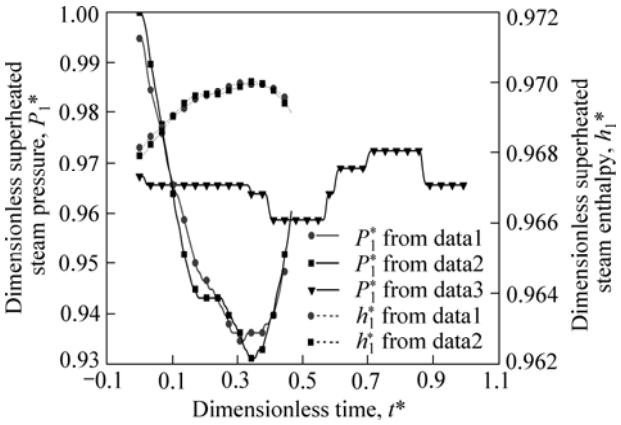


**Fig. 5** Dimensionless superheated steam pressure $P_1^*$ and enthalpy $h_1^*$ of system charge process as a function of dimensionless charge time $t^*$ for three different experiments (data1, data2 and data3)

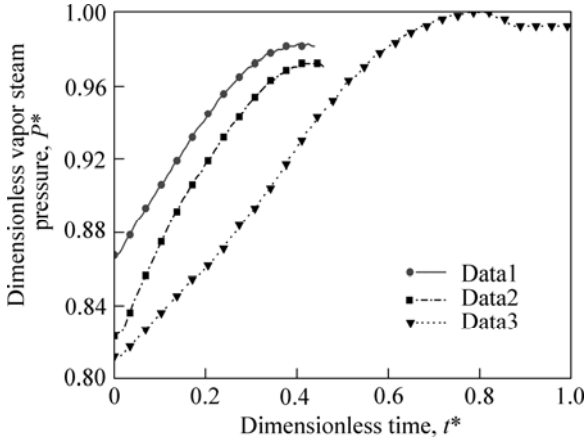


**Fig. 6** Dimensionless steam pressure $P^*$ of steam accumulator as a function of dimensionless charge time $t^*$ for three different experiments (data1, data2 and data3)

### 5.2 Simulation results

To further analyse the relationship between the steam pressure and the steam flow accumulation, Fig. 7 shows the dimensionless steam pressure $P^*$ of steam accumulator as a function of the dimensionless steam flow accumulation $F^*$ for three different experiments and simulation results in an ideal complete mixing condition ($\phi_e \equiv 1$). These results reveal that there is an approximate linear relation between $P^*$ and $F^*$ in an ideal complete mixing condition. But the reality is that the existing of temperature non-uniformity in liquid space brings the less steam flow accumulation than the ideal condition under the same pressure growth of steam accumulator. When the charge time is enlarged to a certain extent (i.e. data3), the differences of steam accumulation between the actual condition and the ideal condition gradually diminish to zero in the end of charge process, that is $\phi_e$=1. Moreover, the effective heating coefficient as a function of $t^*$ for three different experiments (shown in Fig. 8) is also simulated numerically, as well as the time curves of the water average temperature $T_{sub}$.

Figure 9 shows the temperature of vapor steam $T_{sat}$

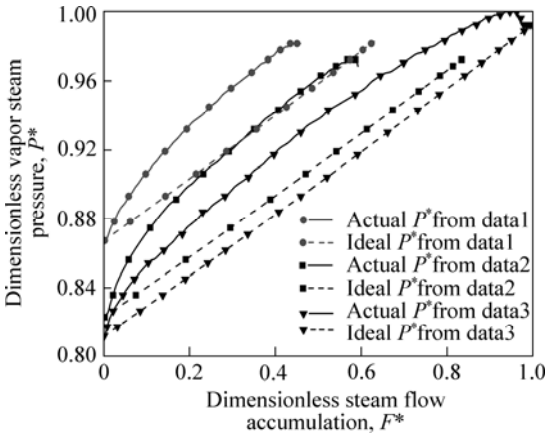


**Fig. 7** Dimensionless steam pressure $P^*$ of steam accumulator as a function of dimensionless steam flow accumulation $F^*$ for three different experiments (data1, data2 and data3) and simulation results in an ideal complete mixing condition

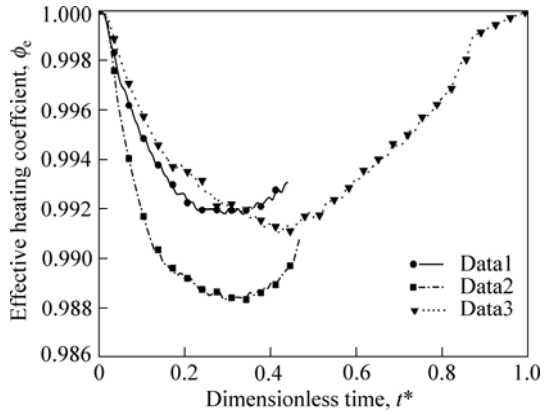


**Fig. 8** Dimensionless effective heating coefficient $\phi_e$ of steam accumulator as a function of dimensionless charge time $t^*$ for three different experiments (data1, data2 and data3)

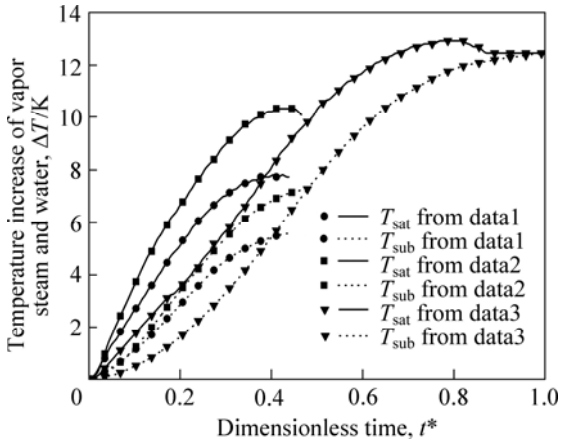


**Fig. 9** Temperature of vapor steam $T_{sat}$ and water $T_{sub}$ from reference point of initial temperature as a function of dimensionless charge time $t^*$ for three different experiments (data1, data2 and data3)

and water $T_{sub}$ from the reference point of initial temperature as a function of $t^*$ for three different experiments.

Figure 9 show that at the beginning of charge process, both $T_{sat}$ and $T_{sub}$ increase sharply, but the former increases even faster. Thus, it confirms that the liquid space still in a sub-cooled state is due to the temperature non-uniformity during the whole charge process. Moreover, a drop of $T_{sat}$ for all the experiments occurs in the late charge process for the temperature heat transfer between the upper vapor space and the lower liquid space. Subsequently, the temperatures of both spaces for data3 even reach the final coordinated one at last, which means a complete thermal mixing in the liquid space.

### 5.3 Evaluation result of system thermodynamic charge performance

Figure 10 shows the average sub-cooled degree $\Delta T_{sub}$ as a function of $t^*$ for three different experiments.

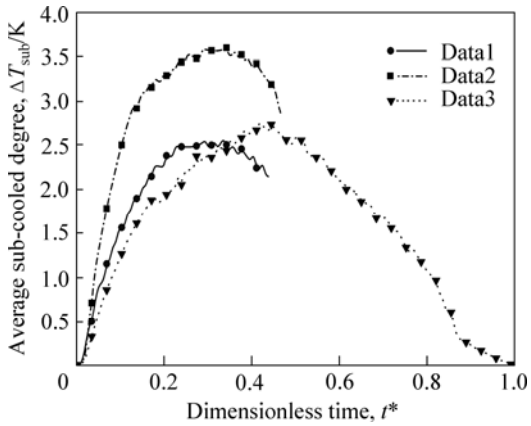


**Fig. 10** Average sub-cooled degree $\Delta T_{sub}$ as a function of dimensionless charge time $t^*$ for three different experiments (data1, data2 and data3)

In the medium-term of charge, $\Delta T_{sub}$ values reach the maximum at 2.6, 3.6 and 2.8, respectively, for data1, data2 and data3 process and then drop to 2.1, 2.9 and 0, respectively, in the end.

Moreover, the presence of linear relation between $\Delta T_{sub}$ and $\phi_e$ can be identified, as shown in Fig. 11, according to Eq. (18).

$$\Delta T_{sub}=308.5\ (1-\phi_e) \tag{18}$$

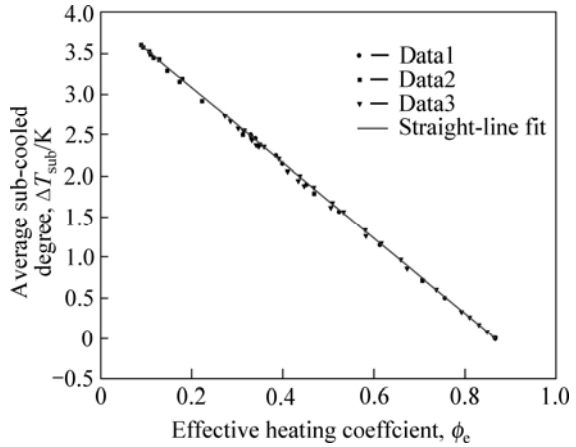


**Fig. 11** Linear relationship between average sub-cooled degree $\Delta T_{sub}$ and effective heating coefficient $\phi_e$ of steam accumulator for three different experiments (data1, data2 and data3)

It is noted from results shown in Fig. 4 and Fig. 10 that the steam flow reflects the average sub-cooled degree qualitatively. At the beginning of charge process for three different experiments, the continuous increasing of un-condensable superheated steam is due to the steam flow rises, which promotes growth of vapor space pressure and ultimately causes an increase of the average sub-cooled degree. Then, later in the charge process, the decrease of average sub-cooled degree for data3 begins with the reduction of the steam flow immediately. However, there are time delays for data1 and data2, and the decrease of average sub-cooled degree is later than the steam flow. Moreover, the time delay for data2 is larger than that for data1 on account of the relatively sharp increase of steam flow. The time delay indicates that certain inertia will exist in the thermal mixing process if the foregoing increase of steam flow is great. Thus, for the existence of inertia in the thermal mixing process, the average sub-cooled degree of data1 and data2 doesn't drop to zero in the end of charge process, that is, still in a sub-cooled state.

Correspondingly, the increasing rate of charge steam flow for data3 is much less than that for data1 and data2, due to the extended period of charge process which can significantly expand the contact time between the charge steam and the liquid water. It provides two advantages for eliminating inertia in the thermal mixing process. On the one hand, more heat energy is released from charge steam into the liquid space, which decreases the water temperature non-uniformity. On the other hand, much less superheated steam quantity flows into the upper vapor space for increasing pressure slowly, which further prolongs the thermal mixing time and decreases the average sub-cooled degree. However, it should be also noted that the charge time is not the longer the better. Over-extension of the charge time will reduce the operating frequency of steam users, thus affecting the use efficiency. Therefore, it needs to weigh up the thermodynamic charge performance and the use efficiency for optimum charge time.

Finally, the charging energy coefficient is calculated by Eq. (4). The charging energy coefficients are 74.6%, 69.9% and 100%, respectively, for data1, data2 and data3.

The above results indicate that the charging energy coefficient related to the end value of the average sub-cooled degree can directly evaluate the thermodynamic charge performance of system. Among the three different experiments, the charging energy coefficient for data3 reaches the highest level in accordance with the above analysis result of average sub-cooled degree that the longer the charge time, the more the heat energy can be absorbed by the liquid water on account of the relatively gentle increase of steam flow. Meanwhile, the comparison for charging energy coefficient between data1 and data2 shows that the differentiation for the charge time between data1 and data2 is not so clear, but the charging energy coefficient for the former is higher than that for the latter for a smaller value of the average sub-cooled degree.

### 5.4 Prediction of average sub-cooled degree

For the existing inertia in the thermal mixing process, as well as the qualitative reflection of the average sub-cooled degree from the charge steam flow, a correlation equation including inertial element is put forward to predict the average sub-cooled degree as

$$C\frac{\mathrm{d}(\Delta T_{sub})}{\mathrm{d}t}+\frac{\Delta T_{sub}}{R}=Q \tag{19}$$

where $C$ and $R$ are the inertia capacity and the scale coefficient, respectively.

Based on the experimental data of $Q$ and $\Delta T_{sub}$ from data2 and data3, $C$ and $R$ as a function of $t^*$ is calculated by Eq. (19) and shown in Fig. 12.

Figure 13 shows the fitting effect of $T_{sub}$ by Eq. (19) for data2 and data3 to the experiment data. The predicting capability of $T_{sub}$ for data1 by Eq. (19) is compared in Fig. 14. Mean and maximum deviations of the predicted results from those by experiment data for data2 are smaller than 6.8% and 10.8%, respectively, which indicates the capability of Eq. (19) to predict the average sub-cooled degree $\Delta T_{sub}$.

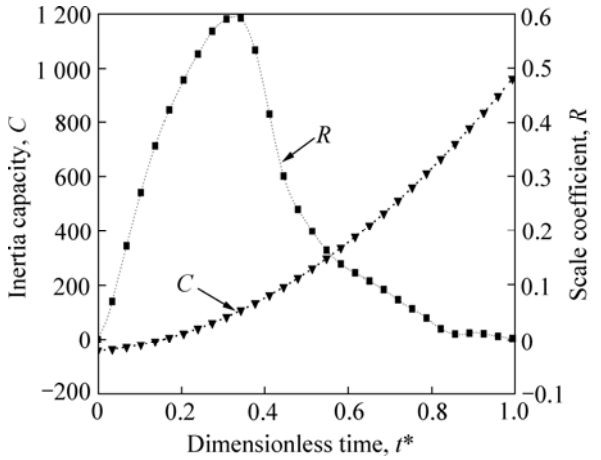


**Fig. 12** Inertia capacity $C$ and scale coefficient $R$ as a function of dimensionless charge time $t^*$

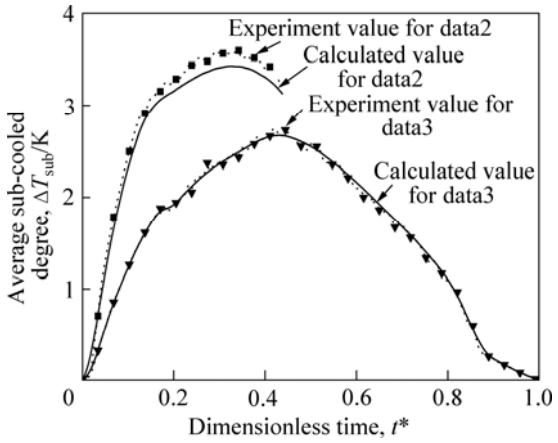


**Fig. 13** Fitting effect of Eq. (19) for data2 and data3

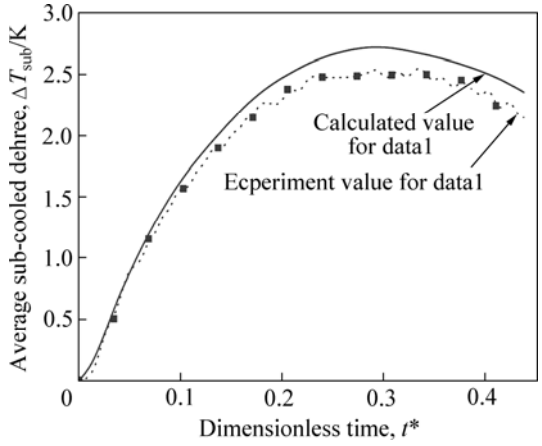


**Fig. 14** Predicting capability of Eq. (19) for data1

## 6 Conclusions

1) By defining the effective heating coefficient that reflects the temperature non-uniformity of liquid water during the charge process, the approximate linear relation between the steam pressure and the steam flow accumulation is obtained in an ideal complete mixing condition.

2) By calculating the average sub-cooled degree of water to evaluate the temperature non-uniformity, the simple quantitative relation between the average sub-cooled degree and the effective heating coefficient is also obtained.

3) By comparing the change rules of the steam flow and the average sub-cooled degree qualitatively, certain inertia will exist in the thermal mixing process if the foregoing increase of steam flow is great. So a correlation equation including inertial element is put forward to predict the average sub-cooled degree and then the capability is proved.

4) Based on the experiments and simulation of system charge process, the charging energy coefficient can be calculated. The results show that the charging energy coefficient can directly evaluate the thermodynamic charge performance of system since it relates to the end value of the average sub-cooled degree. Therefore, in the same charge time condition, the slow increase rate of charge steam flow by adjusting the control strategy of charge valve can effectively increase the charging energy coefficient and therefore improve the thermodynamic charge performance of system. While the increase of the charging energy coefficient by extending the charge time needs the consideration of the operating frequency for steam users.

## References

[1] STEINMANN W D, ECK M. Buffer storage for direct steam generation [J]. Solar Energy, 2006, 80(10): 1277−1282.

[2] ECK M, STEINMANN W D. Direct steam generation in parabolic troughs: First results of the DISS project [J]. Journal of Solar Energy Engineering-Transactions of the ASME, 2002, 124: 134−139.

[3] SANDNES B, REKSTAD J. Supercooling salt hydrates: Stored enthalpy as a function of temperature [J]. Solar Energy, 2006, 80: 616−625.

[4] TAMME R, LAING D, STEINMANN W D. Advanced thermal energy storage technology for parabolic trough [J]. Journal of Solar Energy Engineering-Transactions of the ASME, 2004, 126: 794−800.

[5] DEHGHAN A A, BARZEGAR A. Thermal performance behavior of a domestic hot water solar storage tank during consumption operation [J]. Energy Conversion and Management, 2010, 80: 1277−1282.

[6] FERNA´NDEZ-SEARA J, UHI'A F J, SIERES J. Experimental analysis of a domestic electric hot water storage tank. Part II: Dynamic mode of operation [J]. Applied Thermal Engineering, 2007, 27: 137−144.

[7] ALIZADEH S. An experimental and numerical study of thermal stratification in a horizontal cylindrical solar storage tank [J]. Solar Energy, 1999, 66: 409−421.

[8] GIL A, MEDRANO M, MARTORELL I, LÁZARO A, DOLADO P, ZALBA B, CABEZA L F. State of the art on high-temperature thermal energy storage for power generation. Part 1-Concepts, Materials and Modellization [J]. Renewable and Sustainable Energy Reviews, 2010, 14(1): 31−55.

[9] MEDRANO M, GIL A, MARTORELL I, POTAU X, CABEZA L F. State of the art on high-temperature thermal energy storage for power

generation. Part 2-Case studies [J]. Renewable and Sustainable Energy Reviews, 2010, 14(1): 56−72.

[10] BALDINI A, MANFRIDA1 G, TEMPESTI D. Model of a solar collector/storage system for industrial thermal applications [J]. Int Centre for Applied Thermodynamics, 2009, 12(2): 83−88.

[11] WAGNER W, COOPER J R, DITTMANN A, KIJIMA J, KRETZSCHMAR H J, KRUSE A, MAREŠR, OGUCHI K, SATO H, STÖCKER I, ŠIFNER O, TAKAISHI Y, TANISHITA I, TRÜBENBACH J, WILLKOMMEN T. The IAPWS industrial formulation 1997 for the thermodynamic properties of water and steam [J]. Journal of Engineering for Gas Turbines and Power, 2000, 122(1): 150−182.

[12] CHU Yun-tao, LOU Chun, CHENG Qiang, Zhou Huai-chun. Distributed parameter modeling and simulation for the evaporation system of a controlled circulation boiler based on 3-D combustion monitoring [J]. Applied Thermal Engineering, 2008, 28: 164-177.

[13] HU Ji-min, JIN Jia-shan, YAN Zhi-teng. Fluid-solid coupling numerical simulation of charge process in variable-mass thermodynamic system [J]. Journal of Central South University of Technology, 2012, 19(4): 1063−1072.

[14] ZHOU Nai-jun, ZHOU Shan-hong, ZHANG Jia-qi, PAN Qing-lin. Numerical simulation of aluminum holding furnace with fluid-solid coupled heat transfer [J]. Journal of Central South University of Technology, 2010, 17(6): 1389−1394.

[15] YANG Shi-ming, TAO Wen-quan. Heat transfer [M]. Version 3. Beijing: Higher Education Press, 1998: 206−215. (in Chinese)

[16] LO´PEZ-GONZA´LEZ L M, SALA J M, GONZA´LEZ-BUSTAMANTE J A, MI´GUEZ J L. Modeling and simulation of the dynamic performance of a natural-gas turbine flow meter [J]. Applied Energy, 2006, 83: 1222−1234.

[17] QI Kun-peng, FENG Li-yan, LENG Xian-yin, TIAN Jiang-ping, LONG Wu-qiang. Simulation of quasi-dimensional model for diesel engine working process [J]. Journal of Central South University of Technology, 2010, 17(4): 868−872.

**(Edited by HE Yun-bin)**